Particle Monte Carlo simulation of quantum phenomena in semiconductor nanostructures

Tsuchiya, Hideaki

Ravaioli, Umberto

(Citation)
JOURNAL OF APPLIED PHYSICS,89(7):4023-4029

(Issue Date)
2001-01-18

(Resource Type)
journal article

(Version)
Version of Record

(URL)
https://hdl.handle.net/20.500.14094/90001274

Particle Monte Carlo simulation of quantum phenomena in semiconductor nanostructures

Hideaki Tsuchiya and Umberto Ravaioli[a)]
Beckman Institute, University of Illinois, 405 North Mathews Avenue, Urbana, Illinois 61801

(Received 10 August 2000; accepted for publication 18 January 2001)

Quantum effects in semiconductor devices are usually described in terms of wave functions obtained from the solution of the Schrödinger equation. However, it is difficult to simulate practical devices where clear semiclassical and quantum features coexist, as is the case for nanoscale devices at normal temperatures. We present here a particle description of quantum phenomena derived starting from Wigner's transport formalism, where the dynamics of particles are treated semiclassically, but with an effective force added to account for quantum effects. The resulting model is solved by using a particle Monte Carlo approach, which we apply to describe transport across a single tunneling barrier. Results of the numerical calculations indicate that size quantization and tunneling effects can be well resolved by the combined Monte Carlo/quantum force approach, yielding quantitative agreement with Schrödinger equation results. © *2001 American Institute of Physics.* [DOI: 10.1063/1.1354653]

I. INTRODUCTION

In the usual quantum approaches, the physical state of an individual system is completely specified by a wave function from which the probabilities associated with observable quantities can be derived. In alternative, a particle description of quantum theory has also been examined in terms of the quantum potential, as introduced by Bohm.[1] For instance, it was successfully demonstrated that the quantum potential produces a clear bunching of particle trajectories in the two-slit interference experiment,[2] which is required to obtain the usual fringe intensity pattern. Such a quantum potential approach accounts for the quantum interference effects while retaining the notion of a well-defined particle trajectory. A particle-based approach is very attractive for practical simulation of nanoscale semiconductor devices at normal temperatures, since one would expect to see an admixture of semiclassical and quantum transport features. It is very difficult to resolve the two regions separately and it is even more difficult to formulate a global model approach that covers these regions together. In this article, we propose a particle description of quantum phenomena based upon a quantum force derived from the Wigner's transport formalism.[3–7] The quantum force can be incorporated into the driving force term of the Boltzmann transport equation (BTE),[8,9] which enables us to utilize the well-developed particle Monte Carlo (MC) computational techniques.[10,11] A quantum correction approach has been recently attemped to include the quantum mechanical electron-phonon interaction based upon the concept of Wigner paths in phase space.[12,13] A MC technique was utilized to solve the time evolution of the Wigner function for *spatially homogeneous case*, and it was shown that the collisional broadening is reduced by considering the quantum correction contribution.[12] On the other hand, the main subject of this article is to develop a computational technique to simulate electron transport through *inhomogeneous potential profiles* including abrupt heterointerfaces, where quantum size effects such as tunneling and quantum confinement become important. This technique would really be needed for theoretical description and practical design of multidimensional ultrasmall integrated devices. In this article, to demonstrate the validity of our approach, we present MC solutions of electron transport through a single tunneling barrier consisting of GaAs and AlGaAs. With this simple model, we can carefully identify tunneling and quantum confinement effects, and also can discuss the correspondence with Schrödinger's wave theory in detail.

II. QUANTUM-CORRECTED MONTE CARLO METHOD

The Wigner distribution function, which corresponds to a quantum mechanical distribution function, is generally defined in the space and momentum coordinates[3–7] as

$$f(\mathbf{k},\mathbf{r},t)=\sum_n P_n \int_{-\infty}^{\infty} d\mathbf{u}\,\psi_n\left(\mathbf{r}+\frac{\mathbf{u}}{2},t\right)\psi_n^*\left(\mathbf{r}-\frac{\mathbf{u}}{2},t\right)\mathrm{e}^{-i\mathbf{k}\cdot\mathbf{u}}, \tag{1}$$

where ψ_n represents the state of the system and P_n is the probability of occupying the state n. The transport equation for the Wigner distribution function is given in the form of a modified BTE as[3,14]

$$\frac{\partial f}{\partial t}+\mathbf{v}\cdot\nabla_{\mathbf{r}}f-\frac{1}{\hbar}\nabla_{\mathbf{r}}U\cdot\nabla_{\mathbf{k}}f + \sum_{\alpha=1}^{\infty}\frac{(-1)^{\alpha+1}}{\hbar 4^{\alpha}(2\alpha+1)!}(\nabla_{\mathbf{r}}\cdot\nabla_{\mathbf{k}})^{2\alpha+1}Uf=\left(\frac{\partial f}{\partial t}\right)_C, \tag{2}$$

where U denotes the spatially varying potential energy, represented by using the electrostatic potential ϕ and band discontinuity at heterointerfaces ΔE as $U=q\phi+\Delta E$. Note that $\nabla_{\mathbf{k}}$ operates only on f and $\nabla_{\mathbf{r}}$ operates only on the potential U. Also, $q=-|e|$ for electrons and $q=|e|$ for holes when $|e|$

a)Electronic mail: ravaioli@uiuc.edu

is the elementary charge. In order to account for collisions, we introduce a collision integral describing the time variation of f due to scattering by

$$\left(\frac{\partial f}{\partial t}\right)_C = \frac{1}{(2\pi)^3}\int d^3\mathbf{k}'[W(\mathbf{k}',\mathbf{k})f(\mathbf{k}') - W(\mathbf{k},\mathbf{k}')f(\mathbf{k})]. \tag{3}$$

The functions $W(\mathbf{k}',\mathbf{k})$ represent the scattering rates obtained from Fermi's golden rule. We would include the same types of scattering as in the classical Boltzmann equation. An essential feature of the Wigner formalism is the presence of quantum effects through the inherently nonlocal driving potential, in the expansion of the fourth term on the left-hand side of Eq. (2). In the limit of slow spatial variations, the nonlocal terms disappear and Eq. (2) reduces to the conventional BTE. Here, we indicate with Q_1 the lowest-order quantum correction term obtained by considering only $\alpha = 1$ in the expansion of Eq. (2). The lowest-order term gives a major contribution in the quantum mechanical corrections.[4,8,9] For a two-dimensional problem, Q_1 is written explicitly, as

$$Q_1 = \frac{1}{24\hbar}\left(\frac{\partial^3 U}{\partial x^3}\frac{\partial^3 f}{\partial k_x^3} + 3\frac{\partial^3 U}{\partial x^2 \partial y}\frac{\partial^3 f}{\partial k_x^2 \partial k_y} + 3\frac{\partial^3 U}{\partial x \partial y^2}\frac{\partial^3 f}{\partial k_x \partial k_y^2} + \frac{\partial^3 U}{\partial y^3}\frac{\partial^3 f}{\partial k_y^3}\right). \tag{4}$$

Supposing that the system is relatively close to equilibrium, we introduce for simplicity a displaced Maxwell–Boltzmann distribution function in the correction term, as

$$f(\mathbf{k},\mathbf{r}) = \exp\{-\beta[E_{\mathbf{k}-\overline{\mathbf{k}}} + U(\mathbf{r}) - E_f]\}, \tag{5}$$

where E_f is the Fermi energy, $\beta = 1/k_B T$, $E_{\mathbf{k}-\overline{\mathbf{k}}}$ is the carrier's energy and $\overline{\mathbf{k}}$ indicates the average momentum of the displaced distribution function. The carrier density $n(\mathbf{r})$ is obtained from integration of Eq. (5) over the momentum $\mathbf{k}$, as

$$n(\mathbf{r}) = N_c \exp\{\beta[E_f - U(\mathbf{r})]\}, \tag{6}$$

where N_c indicates the effective density-of-states. We should mention that the earlier simplification is not a limitation of the method, since other numerical improvements such as inclusion of detailed scattering and hot carrier effects can be added in practical simulation by coupling with a Monte Carlo technique described later.

By using these approximations in Eq. (4), we can obtain a two-dimensional quantum-corrected BTE, as (see Appendix)

$$\frac{\partial f}{\partial t} + \mathbf{v}\cdot\nabla_{\mathbf{r}} f + \frac{1}{\hbar}(-\nabla_{\mathbf{r}} U + \mathbf{F}^Q)\cdot\nabla_{\mathbf{k}} f = \left(\frac{\partial f}{\partial t}\right)_C. \tag{7}$$

The quantum effects are incorporated in terms of quantum mechanical driving forces $\mathbf{F}^Q = (F_x^Q, F_y^Q)$ represented by

$$F_x^Q = \frac{\partial}{\partial x}\left[\frac{1}{24}\left(\frac{2\hbar^2}{\mu_x}\frac{\partial^2}{\partial x^2} + \frac{6\hbar^2}{\mu_{xy}}\frac{\partial^2}{\partial x \partial y} + \frac{6\hbar^2}{\mu_{y^2x}}\frac{\partial^2}{\partial y^2}\right)\ln(n)\right], \tag{8}$$

$$F_y^Q = \frac{\partial}{\partial y}\left[\frac{1}{24}\left(\frac{2\hbar^2}{\mu_y}\frac{\partial^2}{\partial y^2} + \frac{6\hbar^2}{\mu_{yx}}\frac{\partial^2}{\partial y \partial x} + \frac{6\hbar^2}{\mu_{x^2y}}\frac{\partial^2}{\partial x^2}\right)\ln(n)\right], \tag{9}$$

where

$$\frac{1}{\mu_x} = \frac{1}{2\hbar^2}\left[3\frac{\partial^2 E_{\mathbf{k}-\overline{\mathbf{k}}}}{\partial k_x^2} - \beta\left(\frac{\partial E_{\mathbf{k}-\overline{\mathbf{k}}}}{\partial k_x}\right)^2\right], \tag{10}$$

$$\frac{1}{\mu_y} = \frac{1}{2\hbar^2}\left[3\frac{\partial^2 E_{\mathbf{k}-\overline{\mathbf{k}}}}{\partial k_y^2} - \beta\left(\frac{\partial E_{\mathbf{k}-\overline{\mathbf{k}}}}{\partial k_y}\right)^2\right], \tag{11}$$

$$\frac{1}{\mu_{x^2y}} = \frac{1}{2\hbar^2}\left[\frac{\partial^2 E_{\mathbf{k}-\overline{\mathbf{k}}}}{\partial k_x^2} - \beta\left(\frac{\partial E_{\mathbf{k}-\overline{\mathbf{k}}}}{\partial k_x}\right)^2\right], \tag{12}$$

$$\frac{1}{\mu_{y^2x}} = \frac{1}{2\hbar^2}\left[\frac{\partial^2 E_{\mathbf{k}-\overline{\mathbf{k}}}}{\partial k_y^2} - \beta\left(\frac{\partial E_{\mathbf{k}-\overline{\mathbf{k}}}}{\partial k_y}\right)^2\right], \tag{13}$$

$$\frac{1}{\mu_{xy}} = \frac{1}{\mu_{yx}} = \frac{1}{\hbar^2}\frac{\partial^2 E_{\mathbf{k}-\overline{\mathbf{k}}}}{\partial k_x \partial k_y}. \tag{14}$$

The physical effect of the quantum forces is to soften the potential variations that the particles feel in the quantum regions where the potential and the carrier density change abruptly. Equations (8) and (9) can be extended to a full-band description of quantum forces if the coefficients given by Eqs. (10)–(14) are evaluated using a complete numerical band structure of $E_{\mathbf{k}}$.

In this article, our goal is to make a comparison between the quantum force approach and Schrödinger's wave theory. We consider a simple transport problem under the assumption of effective mass approximation. When we use the effective masses m_x, m_y and m_z to represent the energy dispersion relation as

$$E_{\mathbf{k}-\overline{\mathbf{k}}} = \sum_{i=x,y,z} \hbar^2(k_i - \overline{k_i})^2/(2m_i), \tag{15}$$

we can derive the following coefficients necessary for Eqs. (8) and (9):

$$\frac{1}{\mu_x} = \frac{-1}{2\hbar^2\beta}[\gamma_x^2(k_x - \overline{k_x})^2 - 3\gamma_x], \tag{16}$$

$$\frac{1}{\mu_y} = \frac{-1}{2\hbar^2\beta}[\gamma_y^2(k_y - \overline{k_y})^2 - 3\gamma_y], \tag{17}$$

$$\frac{1}{\mu_{x^2y}} = \frac{-1}{2\hbar^2\beta}[\gamma_x^2(k_x - \overline{k_x})^2 - \gamma_x], \tag{18}$$

$$\frac{1}{\mu_{y^2x}} = \frac{-1}{2\hbar^2\beta}[\gamma_y^2(k_y - \overline{k_y})^2 - \gamma_y], \tag{19}$$

$$\frac{1}{\mu_{xy}} = \frac{1}{\mu_{yx}} = 0, \tag{20}$$

where $\overline{k_i}$ is again the average momentum of the distribution function and $\gamma_i = \beta\hbar^2/m_i$ $(i = x,y)$. The quantum forces $\mathbf{F}^Q$ under the effective mass approximation are

$$F_x^Q = \frac{\partial}{\partial x}\left\{ \frac{-1}{24\beta}\left[(\gamma_x^2 \Delta k_x^2 - 3\gamma_x)\frac{\partial^2}{\partial x^2} + 3(\gamma_y^2 \Delta k_y^2 - \gamma_y)\frac{\partial^2}{\partial y^2}\right]\ln(n)\right\}, \tag{21}$$

$$F_y^Q = \frac{\partial}{\partial y}\left\{ \frac{-1}{24\beta}\left[(\gamma_y^2 \Delta k_y^2 - 3\gamma_y)\frac{\partial^2}{\partial y^2} + 3(\gamma_x^2 \Delta k_x^2 - \gamma_x)\frac{\partial^2}{\partial x^2}\right]\ln(n)\right\}, \tag{22}$$

with $\Delta k_i = k_i - \overline{k_i}$ $(i = x, y)$.

The momentum components, k_x and k_y, are explicitly included in Eqs. (21) and (22). In a previously proposed quantum force correction,[8,9] the momentum terms were approximated by using the thermal energy as $\hbar^2(k_x - \overline{k_x})^2/2m_x \simeq \hbar^2(k_y - \overline{k_y})^2/2m_y \simeq k_B T/2$, and the corresponding quantum forces were simply represented by

$$F_x^Q = \frac{\partial}{\partial x}\left[\frac{\hbar^2}{12 m_x}\frac{\partial^2 \ln(n)}{\partial x^2}\right], \tag{23}$$

$$F_y^Q = \frac{\partial}{\partial y}\left[\frac{\hbar^2}{12 m_y}\frac{\partial^2 \ln(n)}{\partial y^2}\right]. \tag{24}$$

This formulation differs from the result in Eqs. (21) and (22) in the fact that it gives a force which depends only on the position but not on the momentum of the particles. The simplified quantum forces given by Eqs. (23) and (24) could still be useful when applied to the quantum hydrodynamic models described, for instance, in Refs. 7, 15, and 16.

Based upon Eq. (7), the velocity and the force for particles during the free flights are given, respectively, by the following equations of motion

$$\frac{d\mathbf{r}}{dt} = \mathbf{v}, \tag{25}$$

$$\frac{d\mathbf{k}}{dt} = \frac{1}{\hbar}(-\nabla_{\mathbf{r}} U + \mathbf{F}^Q). \tag{26}$$

The velocity equation is the same as used in the standard MC technique, but the force equation is modified so that the particles evolve under the influence of the classical driving force $-\nabla_{\mathbf{r}} U$, plus the quantum forces $\mathbf{F}^Q$. An advantage of this approach is that the quantum processes such as tunneling are automatically taken into account. In other words, we do not need to solve the Schrödinger equation to calculate the quantum force, a procedure which is indispensable in the original quantum potential framework.[2] Consequently, a full particle description of quantum processes may be attempted following our quantum force approach.

III. SIMULATION RESULTS

We present here the results of computational experiments based upon the inclusion of the equations of motion (25) and (26) in a standard MC simulation with scattering. As a test case, we consider a one-dimensional single tunneling barrier consisting of GaAs and AlGaAs, where tunneling and quantum confinement effects can be carefully identified. In practical calculations, we used

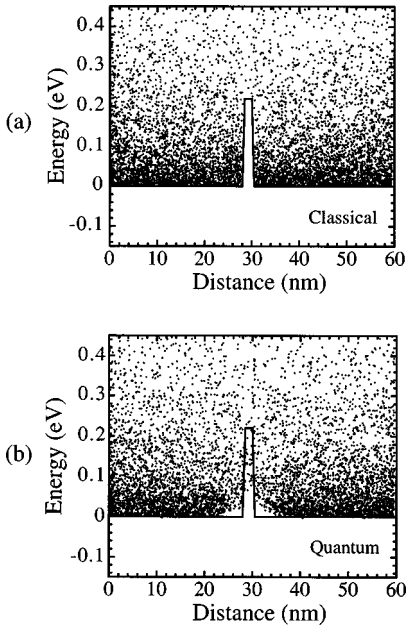

FIG. 1. Electron distributions in space and energy of GaAs/AlGaAs/GaAs single barrier at zero bias voltage using the flatband model. The barrier width is 2.5 nm. (a) corresponds to the classical MC simulation and (b) to the quantum-corrected MC simulation. The conduction band profiles are also plotted with solid lines, and the vertical axis denotes the total electron energy, including the contribution of quantum force (quantum potential).

$$F_x^Q = \frac{\partial}{\partial x}\left\{ \frac{-1}{24\beta}[\gamma_x^2 (k_x - \overline{k_x})^2 - 3\gamma_x]\frac{\partial^2 \ln(n)}{\partial x^2}\right\}, \tag{27}$$

which corresponds to a one-dimensional version of Eqs. (21) and (22). We consider here conduction band discontinuity of 0.22 eV at Γ valley and room temperature (300 K). The doping density in the GaAs electrodes is given as 10^{18} cm^{-3}. As a collisional process, the LO phonon scattering, the acoustic phonon scattering and the ionized impurity scattering are considered. The electron transport at L valley is neglected for simplicity. The extension to the case involving the electron transfer between the two valleys is expected to be possible even in the present quantum approach. To verify the validity of our approach, we first simulated a thermal equilibrium particle distribution without space-charge effects, which allows us to examine the intrinsic tunneling properties through the potential barrier. Figure 1 shows a snapshot of the computed electron distributions in space and energy at zero bias voltage using a simple flatband potential model, and a barrier width of 2.5 nm. Figure 1(a) corresponds to the classical MC simulation without quantum force, and Fig. 1(b) to the quantum-corrected MC simulation with quantum force. For reference, the conduction band profiles are also plotted with solid lines, which corresponds to the potential energy U of Eq. (2). Note that the vertical axis denotes the total electron energy, including the contribution of quantum force.

Comparing the two figures, we can observe two quantum effects in Fig. 1(b). The first one is quantum repulsion by the

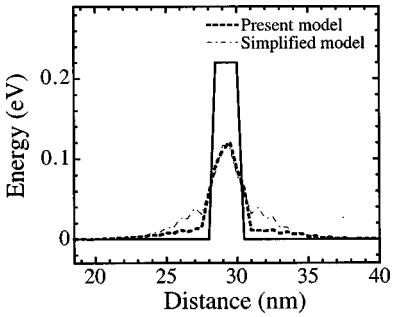

FIG. 2. Effective potential distributions for electrons shown in Fig. 1(b). The dashed line indicates the effective potential variation obtained by averaging over the particles using the quantum correction model of Eq. (27). For comparison, the result obtained with the simplified correction model of Eq. (23) is plotted by the thin dash-dotted line.

potential barrier, where the low energy particles are reflected away from the barrier and very few particles with low energy exist on the left and right of the barrier. The second effect is quantum tunneling through the barrier. In the classical simulation of Fig. 1(a), only the thermally excited electrons with energy larger than the barrier height are found in the barrier region. On the other hand, in the quantum-corrected transport simulation of Fig. 1(b) some tunneling electrons are detected in addition to the thermally excited ones. To clarify the particle tunneling phenomenon observed in Fig. 1(b), the effective potential for the electrons in the simulation is shown in Fig. 2. The quantum force correction depends on the particle momentum and cannot be plotted directly, so we present in Fig. 2 the effective potential distribution obtained by averaging over the particles, using a dashed line. For comparison, the result with the simplified space-dependent model of Eq. (23) is represented by the thin dash-dotted line. The results in Fig. 2 show that the potential barrier is effectively lowered due to the quantum force correction, enabling the particles to penetrate through the barrier. At the same time, the effective potential increases outside the barrier to cause the quantum repulsion mentioned earlier.

To quantify the effect of tunneling in the particle MC simulation, we define a corresponding energy probability derived from the particle distribution. In steady-state, this probability is obtained from a time average of the particles inside the barrier, normalized with that at the left boundary of the device $(x=0)$ as follows:

$$P(E)=\frac{\frac{1}{L_B}\int_{\mathrm{B}} dx\langle f(x,E,t)\rangle}{\langle f(0,E,t)\rangle}, \tag{28}$$

where L_B is the barrier width, $\int_{\mathrm{B}} dx$ denotes spatial integration of the particle distribution function $f(x,E,t)$ over the barrier region, and $\langle\cdots\rangle$ denotes time average. The probability $P(E)$ is designed to represent statistically the particle tunneling properties in a particle-based approach. Figure 3 shows the computed tunneling probabilities as a function of energy at zero bias voltage using the flatband model. The results corresponding to the simulation for barrier width 2.5 nm are given in Fig. 3(a). For comparison, we report also the results for a 4.0 nm barrier in Fig. 3(b). The shaded areas

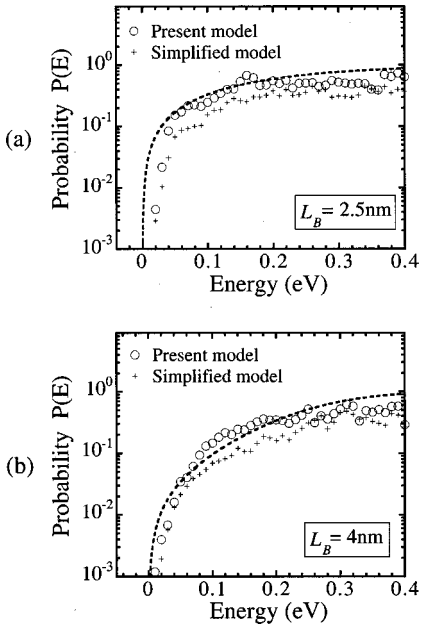

FIG. 3. Computed tunneling probabilities as a function of energy for simulation conditions as in Fig. 1 with barrier width (a) 2.5 and (b) 4.0 nm. The shaded areas indicate the energy range above the barrier ($E>0.22$ eV). The open circles denote the result from the correction model of Eq. (27) and the crosses the result from the simplified correction model of Eq. (23). For comparison, the results from a transfer matrix solution of Schrödinger equation are plotted with the dashed lines.

indicate the energy range above the barrier ($E>0.22$ eV). The open circles denote the result from the present correction model of Eq. (27). For comparison, the results from a transfer matrix solution of Schrödinger equation are plotted with dashed lines. One can see that the results from the quantum-corrected MC and Schrödinger's wave theory are in good agreement, although the MC results fluctuate somewhat in the higher energy region due to the discreteness of the particle energy distribution. The quantum force MC approach describes well both the increasing tunneling probability with energy and the barrier thickness dependence. The earlier results indicate that the statistical probability defined by Eq. (28) is equivalent to the physical tunneling probability at thermal equilibrium. The MC results obtained using the simplified correction model of Eq. (23) are also plotted in Fig. 3 using crosses. The simplified model underestimates the tunneling probability, which should be a consequence of the enhanced quantum repulsion shown in Fig. 2.

For practical device simulation, a nonequilibrium transport analysis with space-charge effects is important. We present next self-consistent MC simulations where Poisson's equation is added and an external bias is applied. Figure 4 shows the computed electron distributions in space and energy at a bias voltage of 0.3 V with barrier width 2.5 nm. Here, Fig. 4(a) corresponds to the classical MC simulation and Fig. 4(b) to the quantum-corrected MC simulation. In Fig. 4(b), we can observe size quantization in the triangular potential well on the left of the barrier. The quantum force correction prevents the electrons from occupying energy states below a certain level, as imposed by the formation of quantized subbands in the triangular potential well. By solv-

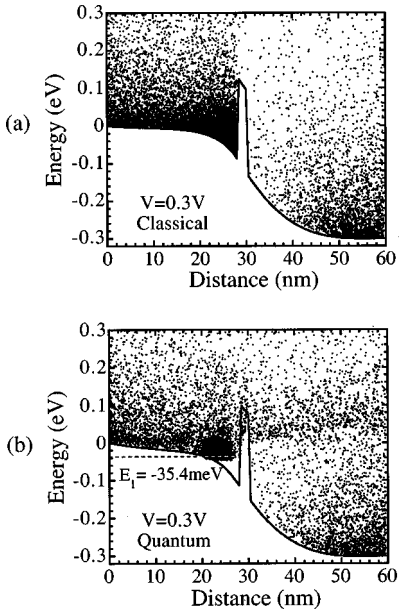

FIG. 4. Self-consistent solutions of electron distribution in space and energy at bias voltage of 0.3 V. The barrier width is 2.5 nm. (a) corresponds to the classical MC simulation and (b) to the quantum-corrected MC simulation. The conduction band profiles are plotted with solid lines, and the vertical axis denotes the total electron energy, including the contribution of quantum force (quantum potential).

ing the Schrödinger equation, we estimated the lowest quantized energy level (E_1) in the triangular potential well as indicated by the dashed line in Fig. 4(b). For this calculation, we used the potential distribution data obtained from the quantum-corrected MC simulation, setting the wave function to be zero at the right barrier interface ($x=30.5$ nm) and the left boundary of the device ($x=0$). The lowest quantized energy level is reasonably close to the bottom of the corrected potential energy for the MC particle distribution in the triangular potential well. Some particles exist slightly below the estimated quantized energies. This should be due to the resonant energy broadening caused by scattering and by tunneling leakage, which are both effectively included in the quantum-corrected MC results. The same quantization behavior was observed for other bias voltages. We can also detect a stream of tunneling particles in the distribution on the right-hand side of the device. This feature was not visible in a similar calculation[9] performed using the simplified correction model of Eq. (23), which does not include the detailed effect of particle momentum.

Figure 5 shows the effective potential distribution averaged over the particles of Fig. 4(b), where the result with the simplified correction model is also plotted. Inside the barrier, the effective barrier height is reduced from the classical one as in Fig. 2. Here, note that the effective potential profile is almost constant in the region between 20.0 and 26.0 nm, which leads to the size quantization of particles found in Fig. 4(b). We can see that the simplified correction model creates a higher repulsive potential in the triangular potential well,[9] and therefore a large difference exists between the two curves near the left interface.

We estimated the tunneling probabilities corresponding to Fig. 4(b) by using Eq. (28), and the results are shown in

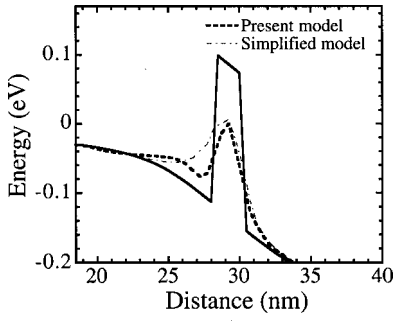

FIG. 5. Effective potential distributions corresponding to Fig. 4(b). The dashed line indicates the effective potential variation obtained by averaging over the particles with the correction model of Eq. (27). For comparison, the result with the simplified correction model of Eq. (23) is plotted by the thin dash-dotted line.

Fig. 6. As before, the open circles denote the result from the present correction model, the crosses the result from the simplified correction model, and the shaded area indicates the energy range above the barrier, where the actual barrier height reduces to about 0.1 eV due to the band bending. The result from a transfer matrix solution of Schrödinger equation, plotted with the dashed line, was obtained using the potential distribution from the quantum-corrected MC simulation. We can see the two major discrepancies between the quantum-corrected MC and Schrödinger's wave theory. One is the tunneling probability oscillation for the lower energy electrons observed in Schrödinger equation result, which is due to the interference effects related to the coherence of electron waves confined in the triangular potential well. The estimates obtained from the quantum-corrected MC results do not show such an oscillatory behavior, which may be due to scattering effects destroying phase coherence, although it is not clear yet to which extent the present particle approach can resolve quantum interference effects. This will be the subject of future investigations. Another discrepancy is the probability decay of the quantum-corrected MC results in the energy range above the barrier. As found in Fig. 4(b), a depletion region is formed on the right of the barrier, and the electrons are extracted from the barrier region quickly by the electric field. This extraction works more effectively for the

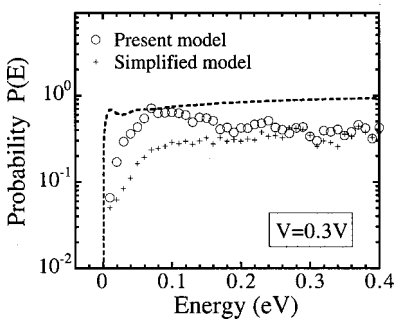

FIG. 6. Computed tunneling probabilities corresponding to Fig. 4(b). The shaded area indicates the energy range above the barrier considering band bending. The open circles denote the result from the correction model of Eq. (27) and the crosses the result from the simplified correction model of Eq. (23). For comparison, the result from a transfer matrix solution of Schrödinger equation is plotted with the dashed line.

higher energy electrons. Therefore, the probability decreases as the electron energy becomes larger than the barrier height. These results mean that the definition of the tunneling probability in Eq. (28) may not be strictly valid in the presence of hot electrons and should only be taken as a guideline for interpretation of the results. We also plotted in Fig. 6 the result from the simplified correction model. Due to the additional repulsion by the hump of effective potential on the left of the barrier (Fig. 5), the probability estimate from the simplified model notably decreases in the energy range below the barrier height ($E<0.1$ eV).

IV. CONCLUSION

We have presented a particle description of quantum phenomena based upon the Wigner's transport formalism, where the dynamics of particles can be treated as in semiclassical Monte Carlo simulation with a nonlocal quantum force correction. The simulation results for transport across a single tunneling barrier indicate that size quantization and tunneling effects can be well resolved by the combined Monte Carlo/quantum force approach, yielding quantitative agreement with Schrödinger equation results. Moreover, our particle-based quantum approach can simulate the admixture of semiclassical and quantum transport features, which is very difficult to describe when starting from a wave description. The particle description of quantum tunneling processes could be useful to explain single electron transport in Coulomb blockade phenomena, where the particle-wave duality of a single electron plays an essential role in the individual tunneling processes. The technique presented in this article should also provide a practical way to include quantum effects in multi-dimensional simulation of ultrasmall integrated devices. It will be the subject of our future investigations to see if the present particle approach can completely resolve quantum interference effects such as in the two-slit interference experiment.

ACKNOWLEDGMENTS

This work was partially supported by the NSF Distributed Center for Advanced Electronics Simulation (DesCArtES), Grant No. NSF ECS 98- 02730 and by the Semiconductor Research Corporation, Contract No. SRC 99-NJ-726. H. T. also would like to thank Professor T. Miyoshi of Kobe University for his kind support and valuable discussions.

APPENDIX: LOWEST-ORDER QUANTUM CORRECTION

By using the displaced Maxwell-Boltzmann distribution function given by Eq. (5), the momentum derivatives of the distribution function f can be transformed, as

$$\frac{\partial f}{\partial k_x}=\frac{\partial f}{\partial E_{\mathbf{k}-\bar{\mathbf{k}}}}\frac{\partial E_{\mathbf{k}-\bar{\mathbf{k}}}}{\partial k_x}=-\beta\frac{\partial E_{\mathbf{k}-\bar{\mathbf{k}}}}{\partial k_x}f, \tag{A1}$$

$$\frac{\partial^2 f}{\partial k_x^2}=-\beta\frac{\partial^2 E_{\mathbf{k}-\bar{\mathbf{k}}}}{\partial k_x^2}f-\beta\frac{\partial E_{\mathbf{k}-\bar{\mathbf{k}}}}{\partial k_x}\frac{\partial f}{\partial k_x}$$
$$=\beta f\left[\beta\left(\frac{\partial E_{\mathbf{k}-\bar{\mathbf{k}}}}{\partial k_x}\right)^2-\frac{\partial^2 E_{\mathbf{k}-\bar{\mathbf{k}}}}{\partial k_x^2}\right], \tag{A2}$$

$$\frac{\partial^3 f}{\partial k_x^3}=\beta\frac{\partial f}{\partial k_x}\left[\beta\left(\frac{\partial E_{\mathbf{k}-\bar{\mathbf{k}}}}{\partial k_x}\right)^2-\frac{\partial^2 E_{\mathbf{k}-\bar{\mathbf{k}}}}{\partial k_x^2}\right]$$
$$+\beta f\left(2\beta\frac{\partial E_{\mathbf{k}-\bar{\mathbf{k}}}}{\partial k_x}\frac{\partial^2 E_{\mathbf{k}-\bar{\mathbf{k}}}}{\partial k_x^2}-\frac{\partial^3 E_{\mathbf{k}-\bar{\mathbf{k}}}}{\partial k_x^3}\right)$$
$$\equiv-\frac{2\hbar^2\beta}{\mu_x}\frac{\partial f}{\partial k_x}, \tag{A3}$$

where

$$\frac{1}{\mu_x}=\frac{1}{2\hbar^2}\left[3\frac{\partial^2 E_{\mathbf{k}-\bar{\mathbf{k}}}}{\partial k_x^2}-\beta\left(\frac{\partial E_{\mathbf{k}-\bar{\mathbf{k}}}}{\partial k_x}\right)^2\right]. \tag{A4}$$

Equations (A2) and (A3) are obtained by using Eq. (A1), with third-order momentum derivatives of $E_{\mathbf{k}-\bar{\mathbf{k}}}$ neglected for simplicity. Similarly, we can express the other momentum derivative terms of Eq. (4) as follows:

$$\frac{\partial^3 f}{\partial k_y^3}=-\frac{2\hbar^2\beta}{\mu_y}\frac{\partial f}{\partial k_y}, \tag{A5}$$

$$\frac{\partial^3 f}{\partial k_x^2\partial k_y}=-\frac{2\hbar^2\beta}{\mu_{x^2y}}\frac{\partial f}{\partial k_y}-\frac{2\hbar^2\beta}{\mu_{xy}}\frac{\partial f}{\partial k_x}, \tag{A6}$$

$$\frac{\partial^3 f}{\partial k_x\partial k_y^2}=-\frac{2\hbar^2\beta}{\mu_{y^2x}}\frac{\partial f}{\partial k_x}-\frac{2\hbar^2\beta}{\mu_{yx}}\frac{\partial f}{\partial k_y}, \tag{A7}$$

where

$$\frac{1}{\mu_y}=\frac{1}{2\hbar^2}\left[3\frac{\partial^2 E_{\mathbf{k}-\bar{\mathbf{k}}}}{\partial k_y^2}-\beta\left(\frac{\partial E_{\mathbf{k}-\bar{\mathbf{k}}}}{\partial k_y}\right)^2\right], \tag{A8}$$

$$\frac{1}{\mu_{x^2y}}=\frac{1}{2\hbar^2}\left[\frac{\partial^2 E_{\mathbf{k}-\bar{\mathbf{k}}}}{\partial k_x^2}-\beta\left(\frac{\partial E_{\mathbf{k}-\bar{\mathbf{k}}}}{\partial k_x}\right)^2\right], \tag{A9}$$

$$\frac{1}{\mu_{y^2x}}=\frac{1}{2\hbar^2}\left[\frac{\partial^2 E_{\mathbf{k}-\bar{\mathbf{k}}}}{\partial k_y^2}-\beta\left(\frac{\partial E_{\mathbf{k}-\bar{\mathbf{k}}}}{\partial k_y}\right)^2\right], \tag{A10}$$

$$\frac{1}{\mu_{xy}}=\frac{1}{\mu_{yx}}=\frac{1}{\hbar^2}\frac{\partial^2 E_{\mathbf{k}-\bar{\mathbf{k}}}}{\partial k_x\partial k_y}. \tag{A11}$$

Notice that the third-order momentum derivatives of the distribution function are expressed in terms of the first-order momentum derivatives in Eqs. (A3), (A5)–(A7). On the other hand, the spatial derivative terms of the potential energy U are represented in terms of the carrier density n by using Eq. (6), as

$$\frac{\partial^3 U}{\partial x^3} = -\frac{1}{\beta}\frac{\partial^3 \ln(n)}{\partial x^3}, \quad \frac{\partial^3 U}{\partial y^3} = -\frac{1}{\beta}\frac{\partial^3 \ln(n)}{\partial y^3} \tag{A12}$$

$$\frac{\partial^3 U}{\partial x^2 \partial y} = -\frac{1}{\beta}\frac{\partial^3 \ln(n)}{\partial x^2 \partial y}, \quad \frac{\partial^3 U}{\partial x \partial y^2} = -\frac{1}{\beta}\frac{\partial^3 \ln(n)}{\partial x \partial y^2}. \tag{A13}$$

By applying these relations to Eq. (4), the lowest-order quantum correction term Q_1 is represented by

$$\begin{aligned} Q_1 = \frac{\partial}{\partial x}\Bigg[\frac{1}{24\hbar}\Bigg(\frac{2\hbar^2}{\mu_x}\frac{\partial^2}{\partial x^2} + \frac{6\hbar^2}{\mu_{xy}}\frac{\partial^2}{\partial x \partial y} \\ + \frac{6\hbar^2}{\mu_{y^2x}}\frac{\partial^2}{\partial y^2}\Bigg)\ln(n)\Bigg]\frac{\partial f}{\partial k_x} + \frac{\partial}{\partial y}\Bigg[\frac{1}{24\hbar}\Bigg(\frac{2\hbar^2}{\mu_y}\frac{\partial^2}{\partial y^2} \\ + \frac{6\hbar^2}{\mu_{yx}}\frac{\partial^2}{\partial y \partial x} + \frac{6\hbar^2}{\mu_{x^2y}}\frac{\partial^2}{\partial x^2}\Bigg)\ln(n)\Bigg]\frac{\partial f}{\partial k_y}. \end{aligned} \tag{A14}$$

The result of Eq. (A14) can be used to formulate the quantum-corrected BTE as given by Eqs. (7), (8), and (9).

[1] D. Bohm, Phys. Rev. **85**, 166 (1952).
[2] C. Philippidis, C. Dewdney, and B. J. Hiley, Nuovo Cimento B **52**, 15 (1979).
[3] E. Wigner, Phys. Rev. **40**, 749 (1932).
[4] H. W. Lee and M. O. Scully, J. Chem. Phys. **77**, 4604 (1982).
[5] W. R. Frensley, Phys. Rev. B **36**, 1570 (1987).
[6] N. C. Kluksdahl, A. M. Kriman, and D. K. Ferry, Phys. Rev. B **39**, 7720 (1989).
[7] J. G. Muga and R. Sala, Phys. Scr. **47**, 732 (1993).
[8] H. Tsuchiya and T. Miyoshi, IEICE Trans. Electron. **E82-C**, 880 (1999).
[9] H. Tsuchiya and T. Miyoshi, Superlattices Microstruct. **27**, 529 (2000).
[10] C. Jacoboni and L. Reggiani, Rev. Mod. Phys. **55**, 645 (1983).
[11] K. Hess, *Monte Carlo Device Simulation: Full Band and Beyond* (Kluwer, Dordrecht, 1991).
[12] A. Bertoni, P. Bordone, R. Brunetti, C. Jacoboni, and N. Sano, Physica B **272**, 299 (1999).
[13] A. Bertoni, P. Bordone, R. Brunetti, and C. Jacoboni, J. Phys.: Condens. Matter **11**, 5999 (1999).
[14] N. Goldsman, C. K. Lin, Z. Han, and C. K. Huang, Superlattices Microstruct. **27**, 159 (2000).
[15] J. R. Zhou and D. K. Ferry, IEEE Trans. Electron Devices **40**, 421 (1993).
[16] M. G. Ancona and G. J. Iafrate, Phys. Rev. B **39**, 9536 (1989).